

Development of μ -PIC as a time-resolved X-ray area detector

Atsushi Takeda,^{a*} Hidehiro Uekusa,^b Hidetoshi Kubo,^a Kentaro Miuchi,^a
Tsutomu Nagayoshi,^a Yuji Ohashi,^b Yoko Okada,^a Reiko Orito,^a Atsushi Takada^a
and Toru Tanimori^a

^aDepartment of Physics, Kyoto University, Kyoto 606-8502, Japan, and ^bDepartment of Chemistry and Materials Science, Tokyo Institute of Technology, 2-12-1 Ookayama, Meguro, Tokyo 152-8551, Japan. E-mail: takeda@cr.scphys.kyoto-u.ac.jp

The application of a two-dimensional micro-pixel gas chamber (μ -PIC) to X-ray diffraction studies, and its performance, are reported. μ -PIC has a 10 cm \times 10 cm detection area, and a fast-readout system for real-time X-ray imaging has been developed. Using the timing of each incoming X-ray measured by μ -PIC, continuous rotation photograph measurements were carried out for a 400 μ m-diameter spherical organic crystal of Ylid (C₁₁H₁₀O₂S), and then diffraction spots were successfully obtained within 2θ of 49°. As a result, good internal agreement factors of 3.7% and 7.0% were confirmed among each of the symmetrically equivalent reflections for exposure times of 3700 s and 98 s, respectively.

© 2005 International Union of Crystallography
Printed in Great Britain – all rights reserved

Keywords: gaseous detector; micro-pattern detector; time-resolved studies.

1. Introduction

In the field of X-ray crystallography, the advent of digital-integration area detectors, such as the imaging plate and the CCD, has dramatically shortened measurement times from a few days to a few hours. On the other hand, photon-counting techniques are considered to be better for obtaining high-quality data, since they provide a more accurate intensity for each diffraction spot; furthermore, they can provide useful information on individual X-ray photons, such as the energy and timing, which are completely lost in integration-area detectors. A typical four-circle diffractometer is the only system that employs a photon-counting detector (scintillation counter); however, it requires quite a long time to measure the necessary diffraction spots owing to its zero-dimensional measurement (a few days). A detector having features of both photon-counting and digital-area detectors is expected to be an ideal area detector in this field. In fact, a multi-wire proportional chamber has been used, but its limitations in terms of high counting rates and fine position resolution have prevented an extension of its use in this field.

Time-resolved X-ray analysis is eagerly awaited in many fields of science. At present, a time-resolved X-ray image can be obtained by combining an integration-area detector and a pulsed X-ray beam derived from synchrotron facilities. If a photon-counting area detector with high counting rates and fine position resolution were to be realised, it would also make possible another approach to time-resolved X-ray analysis. Such a device would provide a movie of diffraction spots from rotating crystals by measuring the timing of each incoming

X-ray photon, which would provide information on the rotation angle of the diffraction spot with a fine angular resolution of less than 0.1°. This new information about the crystal rotation angle of each diffraction spot would enable the removal of most of the background X-rays, and furthermore would dramatically reduce the measurement time since the oscillation of the crystal would be of no use. Also, if periodic measurements become possible for the change or response of a crystal structure, all X-rays measured during many periodic measurements could be folded into one phase of the periodic process with a time resolution of several nanoseconds, and we could measure the dynamical change of a crystal structure directly.

As a candidate for satisfying the above requirements for a photon-counting area detector, two-dimensional pulse-counting detectors, such as the microstrip gas chamber (MSGC), have been studied since the 1990s, and have excellent properties of fine position resolution (~ 100 μ m) and operating capacities under high flux irradiation (Oed, 1988; Tanimori *et al.*, 1996). In fact, the MSGC was applied to X-ray crystallography using a new analyzing method, the 'continuous rotation photograph (CRP) method', as briefly mentioned above. Thus, a rapid analysis of the crystal structure with a measurement time of a few seconds was successfully achieved (Tanimori *et al.*, 1998; Ochi, Uekusa *et al.*, 2001), which was 100 or 1000 times faster than conventional methods, such as using a CCD or four-axis diffractometer. However, MSGCs have the serious problem of discharges, producing critical damage to the detector during practical use. Thus, they can be used only for quite a short measurement time of a few minutes,

and with a low gain of ~ 1000 , both of which causing large systematic errors in the intensities of the measured diffraction spots. Eventually the quality of X-ray crystal structure analyses obtained using the MSGC could not be improved with less than 9% of the internal agreement factor (R_{int}) (Ochi, Nagayoshi *et al.*, 2001).

Furthermore, this detector was examined at SPring-8, one of the largest third-generation synchrotron radiation facilities in the world, in order to realise time-resolved experiments for small-angle X-ray scattering in solution in the millisecond or sub-millisecond time domain; a very wide dynamical range of 10^6 and fast timing resolution of 500 μs were achieved (Toyokawa *et al.*, 2001). Recently, by using this detector, sub-millisecond (250 ms) data acquisition in an X-ray crystal structure analysis was also achieved at the Photon Factory, the high-energy accelerator research organization in Japan (KEK-PF), and the obtained data are currently under analysis.

Thus a photon-counting area detector based on a micro-pattern gas detector such as an MSGC would surely provide many benefits in X-ray crystallography and other kinds of time-resolved experiments, particularly if carried out at synchrotron radiation facilities, providing stable operation was achieved.

In order to overcome the discharge problem, we have developed a micro-pixel chamber (μ -PIC) which is a micro-pattern gaseous two-dimensional imaging detector for real-time X-ray, γ -ray and charged-particle imaging (Ochi, Nagayoshi *et al.*, 2001; Ochi *et al.*, 2002). The μ -PIC has pixel-type anode electrodes surrounded by cathode rings. A gas avalanche occurs around the anode electrodes owing to a strong electric field. On the other hand, the electric field is weaker at the edge of the cathode because of its longer circumference. A detector of this type, the micro-dot chamber (MDOT), was developed earlier (Biagi & Jones, 1995). The MDOT detector, however, has a very thin ($<5 \mu\text{m}$) insulator layer manufactured by integrated circuit technology; it is difficult to obtain a large gas gain owing to distortion of the electric field near the surface of the substrate (Biagi *et al.*, 1997). On the contrary, the μ -PIC has the advantage of a thick (100 μm) substrate manufactured by a quite different technology. These geometrical properties should provide a higher gas gain than the MSGC without any serious discharge problem, so that stable operation at a high gas gain and under high flux irradiation can be realised.

We applied the μ -PIC to X-ray diffraction studies using the CRP method instead of the MSGC, and confirmed the capability of obtaining most of the diffraction spots from one continuous rotation of the sample crystal. In this paper we describe the performance of the μ -PIC for X-ray diffraction studies. In particular, we concentrate on improving the quality of the X-ray crystal structure analysis owing to the high gain and good uniformity of the μ -PIC.

2. μ -PIC

A schematic of the structure of the μ -PIC is shown in Fig. 3 of Takeda *et al.* (2004). The μ -PIC is a double-sided print circuit

board (PCB) with a 100 μm -thick polyimide substrate. An orthogonal cathode and anode strips are formed with a pitch of 400 μm on the front and rear sides of the substrate, respectively. Anode pillars are formed at each centre of a cathode hole through the substrate. By using PCB technology, large-area detectors can, in principle, be mass produced.

We developed a μ -PIC with a 10 cm \times 10 cm detection area (Nagayoshi *et al.*, 2003), which is the same size as that of the MSGC used by Ochi, Uekusa *et al.* (2001). Its electrode structures were optimized using a three-dimensional simulator, so that a high gas gain and good gain uniformity could be achieved (Nagayoshi *et al.*, 2004; Bouianov *et al.*, 2005). The μ -PIC (TOSHIBA SN040223-1) exhibited its maximum gas gain of 16000, and was stably operated at a gain of 6000 for more than 1000 h with an Ar–C₂H₆ (90:10) gas mixture. The gas gain in the whole detection area was uniform within 7% (RMS), as shown in Fig. 8 of Takeda *et al.* (2004).

A data-acquisition system of the μ -PIC, consisting of amplifier-shaper-discriminator (ASD) cards, a position-encoding module and a VME memory module, was developed (Kubo *et al.*, 2003; Miuchi *et al.*, 2003). Signals from the μ -PIC are amplified and discriminated by the ASD cards. Discriminated signals are encoded by the position-encoding module (PEM) of five field-programmable gate arrays (FPGAs) at a clock rate of 20 MHz. The PEM calculates the two-dimensional position of each X-ray by taking the anode–cathode coincidence within one clock pulse, and records it with a few tens of nanoseconds resolution in the memory module. Under 20 MHz operation, the PEM can manage about 7 Mcounts s⁻¹ of randomly incoming X-rays by automatically rejecting accidental double hits within one clock, which is more than ten times better than that obtained by a multi-wire proportional counter. In this way we can realise time-resolved X-ray imaging with the μ -PIC.

A two-dimensional X-ray image of a test chart was obtained with an X-ray generator (Kevex X-Ray CU028, tungsten target). In order to reduce the diffusion of electrons, a Xe–C₂H₆ (70:30) gas mixture at atmospheric pressure was used. Fig. 10 of Takeda *et al.* (2004) shows the obtained X-ray image and the projected X-ray counts along the 0.5 mm slits. Slits of 0.5 mm width can be clearly seen. From the edge image of Fig. 10 of Takeda *et al.* (2004), a two-dimensional position resolution of 120 μm (RMS) was obtained for continuum X-rays of ~ 10 keV using a Xe–C₂H₆ (70:30) gas mixture (Takeda *et al.*, 2004).

3. Measurement by the CRP method and results

We applied the μ -PIC to X-ray diffraction studies using the CRP method. The experimental set-up is shown in Figs. 1 and 2. As an X-ray source, a monochromatic X-ray was generated with a molybdenum target ($K\alpha$: 17.5 keV) and a pyrolytic graphite crystal. The acceleration voltage and tube current were set to be 50 kV and 250 mA, respectively. An organic crystal of Ylid (C₁₁H₁₀O₂S) was mounted on a four-axis goniometer and rotated around the φ axis (0.2 cycles s⁻¹). The detector surface of the μ -PIC was set at 10 cm from the crystal.

The total exposure time was 3700 s. The μ -PIC was placed on a tilt to the X-ray beam at 28.9° , and the centre of the beam was pointed on one edge of the detection area to measure a wide diffraction angle, as shown in Fig. 2. In order to reduce the effect of parallax broadening of the position distributions, a narrow detection depth of 1 mm above the substrate was used. The μ -PIC was filled with an Ar–C₂H₆ (90:10) gas mixture at atmospheric pressure. The absorption efficiency for X-rays in the gas mixture of argon and ethane was lower than that in xenon gas. However, we chose a gas mixture of argon and ethane because the μ -PIC works more stably with it. The μ -PIC was operated with a gain of 3200 and an energy threshold of ~ 4 keV. Since the energy threshold was low enough compared with the energy of the X-ray beam, the fluctuation of the count rate caused by the gain fluctuation over the whole detection area was thought to be negligible.

The observed average counting rate was about 1×10^4 counts s⁻¹ on average in a 10.24 cm \times 10.24 cm effective detection area. The counting-rate variation is shown in Fig. 3 as a function of the elapsed time since the X-ray beam was turned on, where the counting rates were quite stable within 0.7% during the measurement. The maximum count rate of the strongest diffraction spot was 1.6×10^4 counts mm⁻² s⁻¹. This rate was 100 or more times smaller than the capacity of the μ -PIC, including the data-acquisition system, so that no saturation occurred, even for the most intense diffraction spots.

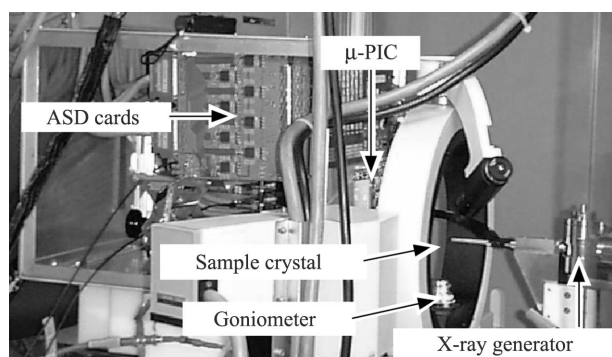


Figure 1
Photograph of the experimental set-up.

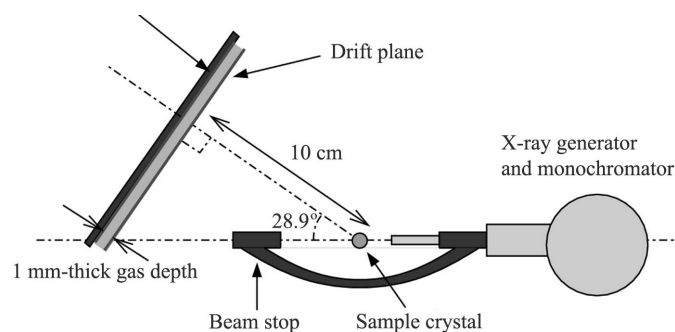


Figure 2
Schematic top view of the experimental set-up used in measurements using the CRP method.

A two-dimensional image of a diffraction pattern of Ylid crystal integrated during a rotation of 360° for the full exposure time (3700 s) is presented in Fig. 4. The maximum measured diffraction angle ($2\theta_{\max}$) was 49° .

The μ -PIC also records the arriving time of X-ray photons using a 20 MHz clock in the PEM with an accuracy of 3.2 ms, where several higher bits of the time counter were only recorded to save the data size. Therefore, the rotation angle of the crystal was precisely measured with a fine angular resolution of 4.2 mrad. Fig. 5(a) shows three-dimensional images obtained from a μ -PIC consisting of two positional and one rotation-angle coordinates. Note that the rotation-angle information enables us to remove the background signals spread uniformly in this space from real spots made by X-ray diffraction of the target crystal.

First, the diffraction spots in this three-dimensional space were searched as follows. The three-dimensional space was divided into small lattices of size 1.6 mm \times 1.6 mm \times 2° , and lattices whose events exceeded 5σ of the background level were chosen as diffraction spots. Here the background level was estimated as an average event included in the 26 adjacent lattices around the spot. This constraint allowed us to use diffraction spots within 2θ of 49° and 25° for exposure times of 3700 s and 98 s, respectively.

Second, in order to obtain an accurate intensity of each diffraction spot, the intensity was recalculated as the total hit

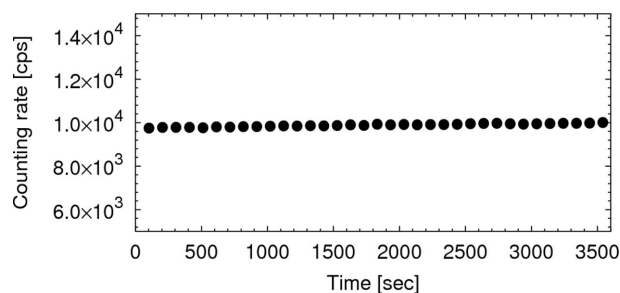


Figure 3
Counting-rate variation as a function of time. The statistical error of each point was within 0.1%.

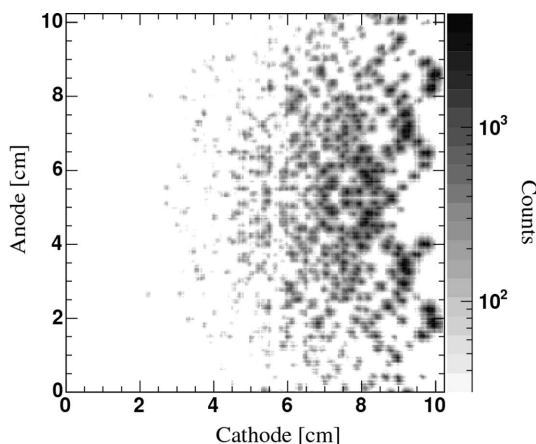
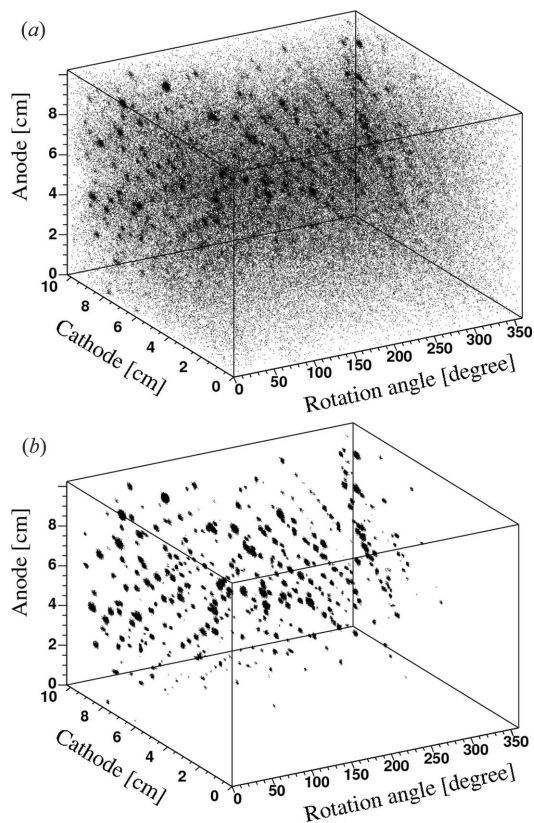


Figure 4
X-ray diffraction image of Ylid integrated over 3700 s. An X-ray beam was pointed on one edge of the detection area (cathode = 10.12 cm, anode = 5.26 cm). The maximum diffraction angle ($2\theta_{\max}$) was 49° .

Table 1

 Exposure times, usable reflections within $2\theta_{\max}$, maximum and minimum hit counts.

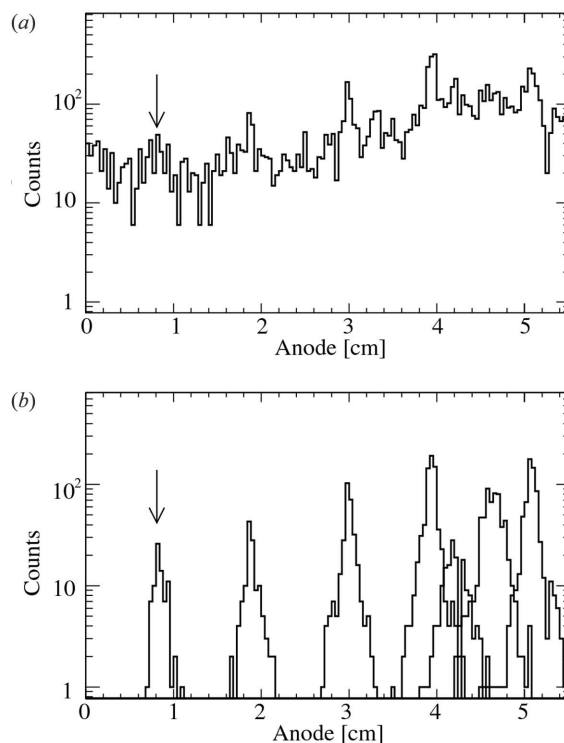
Exposure time (s)	Reflections	$2\theta_{\max}$ ($^{\circ}$)	Maximum counts	Minimum counts
3700	1556	49	1.83×10^5	26
3700	487	25	1.83×10^5	1.94×10^2
98	487	25	4.82×10^3	11


Figure 5

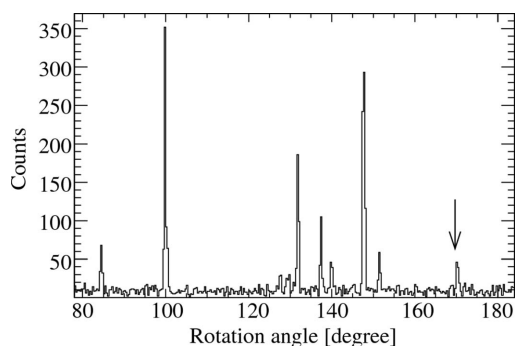
(a) Three-dimensional image (X , Y and rotation-angle coordinates) of X-ray diffraction spots of an organic crystal of Ylid. (b) Similar image after background reduction.

counts included within a newly defined three-dimensional space with a size of $4.0 \text{ mm} \times 4.0 \text{ mm} \times 4^{\circ}$ around the centre of the spot (spot region). Also, the background level corresponding to each spot was recalculated from a larger three-dimensional space of size $12.0 \text{ mm} \times 12.0 \text{ mm} \times 12^{\circ}$ around the centre of the spot, excluding the spot region (background region). When other spot regions were included in the background region, all of those were excluded from the background region. Then, the intensity of each diffraction spot was obtained by subtracting the background level normalized to the spot region from the number of counts in the spot region. By adding the new coordinate of the rotation angle, all spot regions were completely distinguished in the three-dimensional space without any overlapping.

Table 1 summarizes the number of usable diffraction spots, their maximum and minimum hit counts obtained after the background reduction described above for two exposure


Figure 6

Projections of Fig. 4 onto the Y (anode) coordinate (a) before and (b) after applying background reduction using the rotation-angle information. The arrows in the figures are explained in the text.


Figure 7

Event plot *via* the rotation-angle coordinate. The arrow is explained in the text.

times, and 2θ . Fig. 5(b) shows the same figure as that in Fig. 5(a), but after background reduction using the rotation-angle information was applied.

Fig. 6 explains the validity of this background-reduction method for part of the data, which corresponded to an exposure time of 98 s. The projection of Fig. 4 onto the Y (anode) coordinate is shown in Fig. 6(a), where many diffraction spots and a continuous background can be seen. Fig. 7 shows a plot of the events of Fig. 6(a) as a function of the rotation-angle coordinate. Clear peaks concentrated within 1° can be found, which indicates that the background away from the peak can be easily removed using the rotation-angle information. Fig. 6(b) shows Fig. 6(a) after applying background reduction using the rotation-angle information. There

remains very little background below the clear peak. In particular, a faint peak, indicated by the arrow in Fig. 6(a), can be improved as a sharp peak, indicated by the arrow in Fig. 6(b), using the rotation-angle information indicated by the arrow in Fig. 7. Several overlaps of the diffraction peaks appearing in Fig. 6(b) are due to integration along the rotation-angle coordinate, and are perfectly separated, as shown in Fig. 5(b). Owing to this background reduction, the sensitivity for a faint diffraction spot was improved by about ten times. The X-ray counts of the diffraction spot were derived from the total events within a circle of 3σ of the position resolution around the centre position of the spot, while the number of background events was estimated from the events distributed uniformly over the region near to the spot. Finally, the ratio of the most intense count to the least intense reached almost 10^4 , as described in Table 1. The position and angular resolutions (RMS) of the diffraction spot at $2\theta = 25^\circ$ for one 17.5 keV X-ray photon are about 0.6 mm and 3.7 mrad, respectively.

In this experiment, the position resolution was mainly determined by the spatial resolution of the μ -PIC for argon gas, the parallax and the crystal size broadening. The broadenings owing to the latter two components were estimated to be 150 μm and 200 μm , respectively, and hence the first component was calculated to be 550 μm . The RMS of the range of the emitted electron by the photoabsorption process for a 17.5 keV X-ray is ~ 1 mm. Taking account of the projection factor to the detector plane of $1/\sqrt{2}$ and the averaging effect by the number of primary electrons generated along the photoelectron, this spatial resolution of 550 μm is reasonable.

On the other hand, the angular resolution was determined by the monochromatic feature of the X-ray beam, and the defect of the crystal. In this experiment the dispersion of the monochromator was estimated to be about 3.7 mrad (RMS), which is consistent with the above-mentioned angular resolution. Therefore, if xenon gas (spatial resolution of 120 μm) was used, this ratio of the most intense count to the least intense would be improved by several times in principle.

Fig. 8 shows diffraction spots in reciprocal space. The integrated intensities (I_{hkl}) were calculated from the X-ray counts of the spot and background areas, and the Lorentz and polarization correction were applied for each reflection.

As a result, the number of obtained reflections was 1556 up to a diffraction angle of 49° for an exposure time of 3700 s, which includes 331 unique reflections. A good internal agreement factor (R_{int}) of 3.7% was obtained among each of the symmetrically equivalent reflections. Also, for a narrower 2θ of 25° , R_{int} values of 3.7% and 7% were obtained using 487 reflections, including 90 unique reflections for exposure times of 3700 s and 98 s, respectively.

Fig. 9 shows a comparison of the intensities of the diffraction spots within 2θ values of 25° , obtained using the μ -PIC for an exposure time of 98 s, with the same diffraction spots measured by the CCD detector (SMART CCD by Siemens), which is commonly used for crystallography, for an exposure time of ~ 3 h. Both results are very consistent, except for a few points.

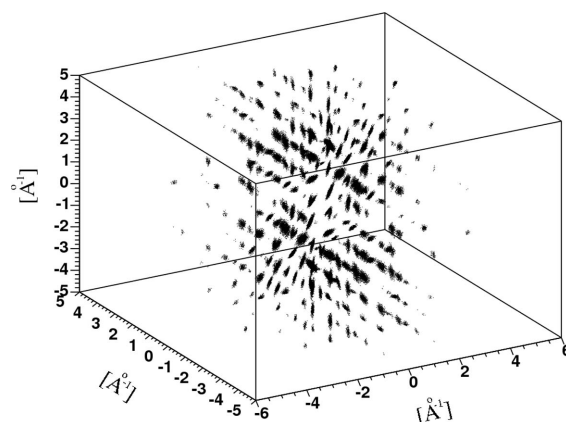


Figure 8 Reciprocal lattice image obtained using the μ -PIC.

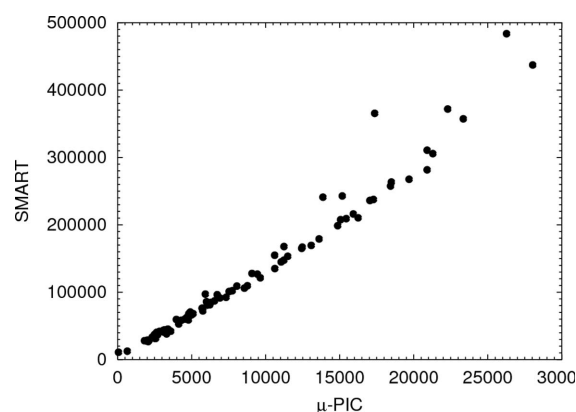


Figure 9 Comparison of the intensities of the diffraction spots obtained using the μ -PIC for an exposure time of 98 s with those obtained using the CCD detector (SMART CCD by Siemens) using another crystal for an exposure time of ~ 3 h.

4. Discussion

CRP measurements with the μ -PIC were carried out using an organic crystal of Ylid. Although the limitation of 2θ coverage within 49° prevented us from analyzing the crystal structure, a good R_{int} of 3.7% was obtained among each of the symmetrically equivalent reflections for an exposure time of 3700 s. Also, even for a shorter exposure time of 98 s, an R_{int} of 7.0% was achieved. Typical counting rates of the diffraction spots for exposure times of 3700 s and 98 s were several times 10^2 and 10^3 counts s^{-1} , respectively, of which the statistical fluctuations are consistent with those of R_{int} . As mentioned in §3, new information concerning the rotation angle enabled us to dramatically reduce the systematic errors owing to the background X-rays and pile-up of the diffraction spots. Indeed, it indicates that the error is mainly due to the statistics of the hit count of the diffraction spots, which are obviously due to the feature of pulse counting. Typical errors of the imaging plate and the CCD are about 3%, which are mainly due to the systematics of the detectors.

In this experiment, X-rays were generated by 50 kV and 250 mA operation. Even the burst rate of the strongest

diffraction spot among these measurements was at most 3.6×10^5 counts s^{-1} for the whole detector, or 1.6×10^4 counts $mm^{-2} s^{-1}$. Both are 100 or more times smaller than the maximum capacities of the data-acquisition system (7 Mcounts s^{-1} for the 20 MHz clock of the PEM) and μ -PIC ($\geq 10^7$ counts $mm^{-2} s^{-1}$) (Ochi *et al.*, 2002). In addition, a 30 cm \times 30 cm large-area μ -PIC and a 100 MHz PEM are being developed, which will provide a wider coverage of 2θ , and an increase by five times in the data-handling capability. Thus, this method seems to be promising for obtaining not only a shorter exposure time for time-resolved analysis but also high-quality data with less than 1% of R_{int} by increasing the pulse-counting ability.

Furthermore, under intense synchrotron radiation sources X-ray structure analyses based on this method are expected to be performed 100 or more times faster, which would enable time-resolved crystal structure analysis in the millisecond or sub-millisecond domain using a monochromatic X-ray beam. Also, as mentioned in the *Introduction*, such photon-counting area detectors will dramatically improve the performances of several kinds of time-resolved X-ray experiments in the microsecond or nanosecond domain under intense synchrotron radiation sources.

We thank Dr Ochi for his support in developing the analysis method. This work is supported by a Grant-in-Aid from the 21st Century COE 'Center for Diversity and Universality in Physics'; a Grant-in-Aid in Scientific Research of the Japan Ministry of Education, Culture, Science, Sports, Technology.

References

- Biagi, S. F., Bordas, J., Duxbury, D. & Gabathuler, E. (1997). *Nucl. Instrum. Methods*, **A392**, 131–134.
- Biagi, S. F. & Jones, T. J. (1995). *Nucl. Instrum. Methods*, **A361**, 72–76.
- Bouianov, M., Bouianov, O., Nagayoshi, T., Kubo, H., Miuchi, K., Orito, R., Takada, A., Takeda, A. & Tanimori, T. (2005). *Nucl. Instrum. Methods*, **A540**, 266–272.
- Kubo, H., Miuchi, K., Nagayoshi, T., Ochi, A., Orito, R., Takada, A., Tanimori, T. & Ueno, M. (2003). *Nucl. Instrum. Methods*, **A513**, 94–98.
- Miuchi, K., Kubo, H., Nagayoshi, T., Ochi, A., Orito, R., Takada, A., Tanimori, T. & Ueno, M. (2003). *IEEE Trans. Nucl. Sci.* **NS-50**, 825–830.
- Nagayoshi, T., Kubo, H., Miuchi, K., Ochi, A., Orito, R., Takada, A., Tanimori, T. & Ueno, M. (2003). *Nucl. Instrum. Methods*, **A513**, 277–281.
- Nagayoshi, T., Kubo, H., Miuchi, K., Orito, R., Takada, A., Takeda, A., Tanimori, T., Ueno, M., Bouianov, O. & Bouianov, M. (2004). *Nucl. Instrum. Methods*, **A525**, 20–27.
- Ochi, A., Nagayoshi, T., Koishi, S., Tanimori, T., Nagae, T. & Nakamura, M. (2001). *Nucl. Instrum. Methods*, **A471**, 264–267.
- Ochi, A., Nagayoshi, T., Koishi, S., Tanimori, T., Nagae, T. & Nakamura, M. (2002). *Nucl. Instrum. Methods*, **A478**, 196–199.
- Ochi, A., Uekusa, H., Tanimori, T., Ohashi, Y., Toyokawa, H., Nishi, Y., Nishi, Y., Nagayoshi, T. & Koishi, S. (2001). *Nucl. Instrum. Methods*, **A467–468**, 1148–1151.
- Oed, A. (1988). *Nucl. Instrum. Methods*, **A263**, 351–359.
- Takeda, A., Kubo, H., Miuchi, K., Nagayoshi, T., Okada, Y., Orito, R., Takada, A., Tanimori, T., Ueno, M., Bouianov, O. & Bouianov, M. (2004). *IEEE Trans. Nucl. Sci.* **NS-51**, 2140–2144.
- Tanimori, T., Aoki, S., Nishi, Y. & Ochi, A. (1998). *J. Synchrotron Rad.* **5**, 256–262.
- Tanimori, T., Ochi, A., Minami, S. & Nagae, T. (1996). *Nucl. Instrum. Methods*, **A381**, 280–288.
- Toyokawa, H., Fujisawa, T., Inoko, Nagayoshi, T., Nishi, Y., Nishikawa, Y., Ochi, A., Suzuki, M. & Tanimori, T. (2001). *Nucl. Instrum. Methods*, **A467–468**, 1144–1147.